Formation of the Enorama Salt Diapir

Weld, Flinders Ranges South Australia

Thesis submitted in accordance with the requirements of the University of Adelaide for an Honours Degree in Geology

David Telfer

October 2013

THE UNIVERSITY of ADELAIDE

FIELD STUDY AND DIAPIR FORMATION MODELLING OF A SALT DIAPIR WELD FLINDERS RANGES, SOUTH AUSTRALIA

(RUNNING TITLE) ENORAMA SALT WELD, FLINDERS RANGES

ABSTRACT

The Adelaide Geosyncline is a basin composed of Neoproterozoic and Cambrian sediments that were deformed by the Cambro-Ordovician Delamerian Orogeny. Early stages of basin development included the deposition of Willouran age (early Cryogenian) evaporites, which have formed the principal detachment surface for the Delamerian Orogen in the Flinders Ranges. Differential loading of the salt units has resulted in formation of several salt diapirs. This study looks into the development of the Enorama and Oraparinna Diapirs. Small scale (1.5 x 1.5km) field mapping project was undertaken and led to the discovery of Pualco Tillite in direct contact with the diapir indicating early Sturtian initiation of diapirism. Differentiation of diapir textures and distribution and composition of clasts indicates that mobility within the diapiric breccia was not uniform during growth of the younger Enorama Diapir. This is particularly due to the Brecciated Red Shale (BRS) which has been described for the first time within the diapir body in this location. It indicates a zone of high mobility relative to the bulk of the diapiric breccia. The BRS is only evident in the activity of the second minibasin to the south, after the active depocentre has moved from the north.

KEYWORDS

Salt Tectonics, salt, diapir, weld, Flinders Ranges, diapir rafts, differential load

TABLE OF CONTENTS

LIST OF FIGURES AND TABLES PAGE

INTRODUCTION

Deformation structures associated with salt diapirism and subsequent salt withdrawal have been modelled in laboratory simulations and compared to seismic analogues in the Gulf of Mexico (Rowan and Vendeville 2006), Angola (King et al. 2012), the Zagros Mountains of Iran (Motamedi et al. 2011, Vendeville 1992a), Oman (Schoenherr et al. 2010, Claringbould et al. 2013) and outcrop analogues in the Flinders Ranges, South Australia (SA) (Rowan and Vendeville 2006).

Composite Halokinetic sequence stratigraphy describes strata orientations adjacent to diapirs in order to determine relative growth rates of the diapir and the rate of sedimentation (Figure 1) (Giles 2012). Halokinesis structures have been measured and compared on both flanks of the diapir weld, and indicate that diapirism occurred syn-depositional in the later stages (Lemon 1988), and that flip flop tectonics structures (Quirk 2012) are present.

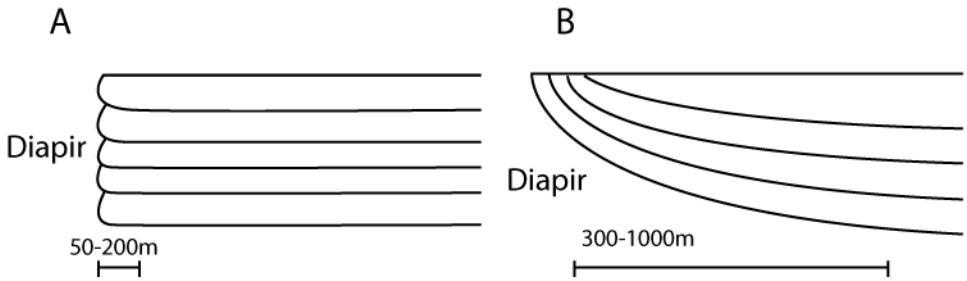

Figure 1 Composite Halokinetic Sequence Stratigraphy (CHS) (Giles 2012). A) Hook CHS. Discordant bedding planes adjacent to the diapir indicate pulses of diapirism disrupting the surface. B) Wedge CHS Concordant bedding planes adjacent to the diapir indicate diapirism acting on deep sediments in a ductile manner (Giles 2012).

Some species of diapirs have been modelled and documented to have minibasins that switch from one side of the salt body to the other through the course of salt movement

and basin filling (Quirk 2012). This change in depocentre invariably leads to a change in the character of salt movement, and therefore shape of the subsequent diapir (Ferrer 2012). Salt diapirs occur in environments where salt and other evaporites are overlain by sediments. Salt, and hence evaporite lithologies have a very low yield strength, therefore when a differential load is placed upon them, piercing of overlying strata (diapirism) can occur (Jackson et al. 1994).

Sediments adjacent to the Enorama, Oraparinna and Blinman diapirs in the Flinders Ranges South Australia (SA) have been described as syn-depositional (Lemon 1985, Lemon 1988), that diapir growth was occurring while the adjacent sediments were being deposited. It has been shown that diapirism was a result of differential sedimentary loading, gravity sliding and spreading in an extensional tectonic environment (Dyson 1996, Dyson 1998, Dyson 2004, Jackson and Vendeville 1994). Further tectonic influence has been documented in seismic data through basin inversion due to reactivation of basement (Backé et al. 2010).

The weld connecting the Enorama and Oraparinna diapirs shows mainly concordant wedge geometries which indicate that submarine carbonate sedimentation in the area was occurring faster than diapirism (Lemon 1985, 1988). Various faults have been documented and interpreted in association with the weld and salt withdrawal; the Bunkers Graben, is a large collapse structure to the east of the Oraparinna Diapir (Dalgarno 1965). A thrust has been interpreted along the northern flank of the weld connecting the diapirs (Lemon 1988) and three parallel transpressional faults oriented parallel to, and located within the weld have been identified (Clarke 1994). Overall

these structures demonstrate westward movement during the Cambro-Ordovician Delamerian Orogeny. This trend is consistent with the overall vergence of the orogen (Preiss 2000).

In this study, I investigate the formation of a secondary diapir (The Enorama Diapir), which formed in a structural weakness that formed due to the growth of a primary diapir (The Oraparinna Diapir). Mapping is undertaken to demonstrate 1) the nature and characteristics of diapirism in relation to surrounding submarine sediments, and 2) the manner of subsequent secondary diapirism and salt withdrawal shown through stratigraphic relationships.

Field mapping focussed on the outcrops of the weld between the Enorama and Oraparinna Diapirs. A 1.5 x 1.5 km scale area was chosen to study sediments adjacent to the diapir in more detail including; thickness, distortion of bedding planes and internal character. This field area was chosen in order to do a more focused small scale study targeting the geometry and structures associated with the weld between the Oraparinna and Enorama diapirs, in order to build on previous work (Dalgarno 1965, Lemon 1988). Additionally the internal character of the diapir was documented, both the clasts and texture of the diapiric breccia and the distribution and composition of diapiric rafts. Using this data, this study aims to define the style of diapir growth in context of the tectonic events acting on and within the Adelaide Geosyncline.

GEOLOGICAL SETTING

Sediments forming the Adelaide Geosyncline (Basin) were deposited in the Neoproterozoic, and were deformed by the Cambrian-Ordovician Delamerian Orogeny (Priess 1993). The area affected by the Delamerian Orogeny extends from Kangaroo Island in the south, to the northern Flinders Ranges (Figure 2) and Willouran Ranges in

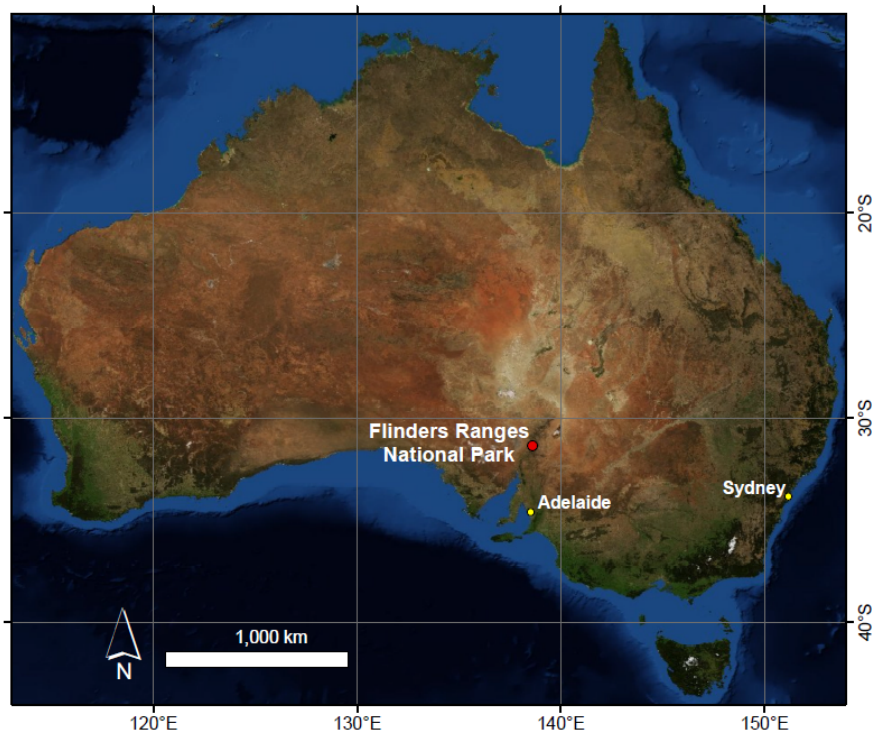

Figure 2 Location map for the Flinders Ranges National Park on the Australian Continent

the north (Drexel 1995). To the north-west, the Adelaide Geosyncline is bounded by the Stuart Shelf, and to the south-west the Gawler Craton (Drexel 1995). To the east the Adelaide Geosyncline is bounded by the Curnamona Craton (Figure 3) (Priess 1993). The Delamerian has been divided into three separate stages of deformation; the first was north-west south-east shortening, followed by north south shortening, and finally a second stage of north-west to south-east shortening (Preiss 2000).

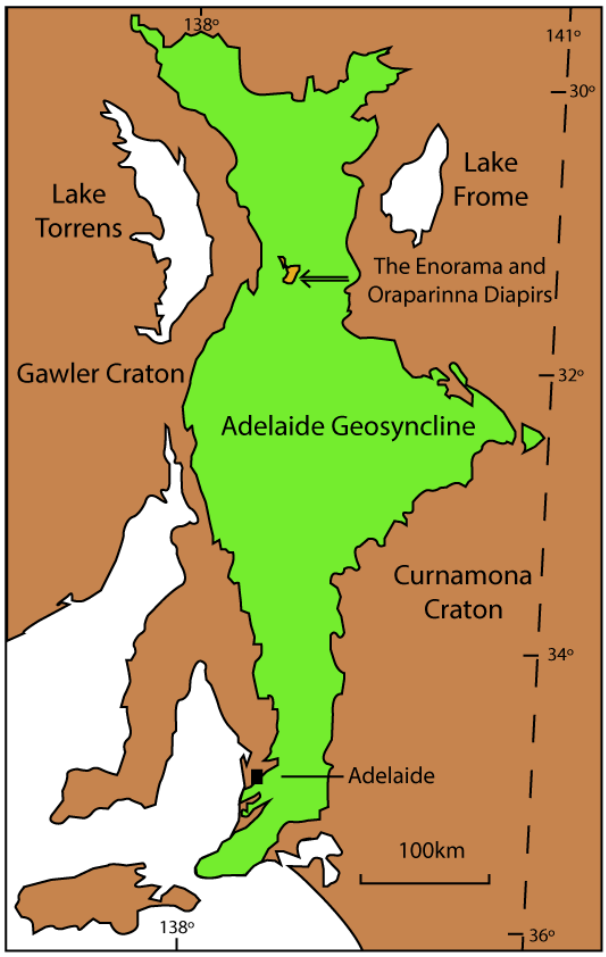

Figure 3 The Adelaide Geosyncline and adjacent cratons

Diapir structures formed during the Delamerian Orogeny from Willouran age evaporite sediments of the Cryogenian age Adelaidean Group (Lemon 1988). Material from these diapirs shows characteristics of both the Curdimurka and Arkaroola subgroups (Figure 4), indicating that in the course of transportation, significant mixing and distortion has occurred (Dyson 1996). The depositional environment of the Curdimurka Subgroup (Figure 4) has been described as a playa lake with associated sabkha (Lemon 1988). This is consistent with shale and sand observed in the diapiric breccia, and high levels of salt (Jackson et al. 1994). Diapirism is present widely across the Adelaide Geosyncline and has been extensively mapped and documented (Dalgarno 1965,

Dalgarno 1966, Dyson 1996, Dyson 1998, Dyson 1999, Dyson 2004, Kernen 2012, Lemon 1985, Lemon 1988, Mooney 1981, Mount 1975).

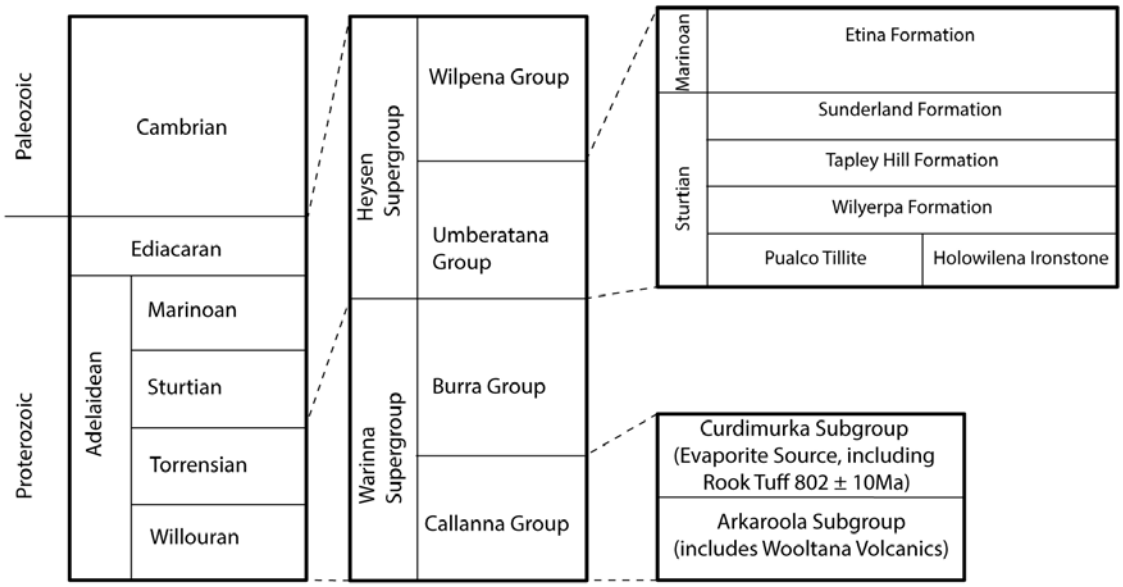

Figure 4 Stratigraphy of the Central Flinders Ranges in the vicinity of the Enorama Diapir, The Curdimurka and Arkaroola Subgroups form the diapiric breccias of the Enorama and Oraparinna Diapirs. Formations of the Umberatana Group are the units adjacent to these diapirs (Figure 9) (Priess 1993, Fanning 1986)

Evaporites are sediments with a significant quantity of crystallized salts, and can be a product of both terrestrial and marine environments (Archer 2012, Jackson et al. 1994, Mount 1975, Vendeville 1992b). Due to the low yield strength of salt (i.e. evaporite lithologies), it is likely that diapirism began while evaporites were still being deposited due to an uneven overlying sedimentary load (Lemon 1988). Differential loading was also found to be the cause for the earliest stages of diapir formation in the Willouran Ranges (Dyson 2004).

The current surface expression of these diapirs in the Flinders Ranges is in the form of salt leached diapiric breccias (Lemon 1988). These diapir breccias have been

documented having no remaining salt (Lemon, 1988). An extensive leaching process has distorted all but the most recent of deformation fabrics. Hence the majority of the work on Flinders Ranges salt diapirs has been undertaken on the surrounding strata (Dyson 1996, Dyson 1998, Dyson 1999, Dyson 2004, Kernen 2012, Lemon 1985, Lemon 1988, Mooney 1981, Mount 1975, Rowan and Vendeville 2006)

The following lithologies are from the Umberatana Group of the Sturtian Glaciation (Table 1). Formations encountered in this study are described below as published (Priess 1993, Preiss 2000, Preiss 1987, Lemon 1988, Fanning 1986, Clarke 1994) with additional observations from the field. All Formations form the Umberatana Group, with the exception of the diapiric breccia lithologies, which come from the Willouran age Curdimurka and Arkaroola Subgroups.

Table 1 Names, ages and descriptions (published and additional field observations) of Formations within the Enorama and Oraparinna Diapirs (Figure 8) (Willouran age) and adjacent to (Umberatana Group) (Preiss 1987, Lemon 2011, Dalgarno 1966, Dalgarno 1965, Clarke 1994).

Name	Published description	Additional characteristics observed in the field
Etina Formation *(Late Sturtian – Early Marinoan)*	Intercalated formation of grey oolitic limestones, dolomitic siltstones and shales. The limestones are composed of a high quantity of coarse sand grains giving a gritty texture. Ooids are spherical and ellipsoidal.	Imbricated clasts of sandy limestone form layers, increasing in size with proximity to the diapir (up to 4mm) (Figure 5)
Sunderland Formation *(Late Sturtian)*	Fine grained calcareous siltstone and shale, grey to green in colour(Clarke 1994). The base is composed of conglomerate and oolitic limestone. Slumped bedding has been identified at the top of the formation. Previously this formation was included within the Tapley Hill Formation.	Homogenous grey green colour, with significant resistance to weathering. Commonly crops out on topographic highs.
Tapley Hill Formation *(Late Sturtian)*	Dark bluish grey, slightly calcareous siltstone with fine pyrite grains. The formation coarsens upward with alternating pale and dark laminations, which are caused by organic pigmentation.	Coarse sandstones define this Formation in the field area. Shale units are either covered by regolith or absent.

Wilyerpa Formation *(Middle Sturtian)*	Composed of silts and mudstones that alternate with sandstone layers. Small bands (5-10cm) bands of arkose erratics are present. The sandstones are massive and laterally continuous.	No additional features found
Holowilena Ironstone *(Early Sturtian)*	Dominated by purple and red hematite siltstone and red shale. It includes minor lenses of dolomite quartzite pebbles. Silt units are finely laminated and occaisionally have small-scale cross beds. Discontinuous quartzite layers occur within shale units and are generally no greater than 1m thick. Holowilena Ironstone that crops out in the area east of the Oraparinna Asbestons Mine has been documented with abundant erratics of stromatolitic dolomite and quartzite and bands of jasper and jasper breccia.	Interbedded zones of red, yellow, white and green layers on a 5 – 10cm scale. These are generally observed in the first few metres near the base of the dolomite layer at the boundary of the diapir. These layers reappear again near the boundary with the Wilyerpa Formation. Sand lenses include subangular clasts of sandstone of 1 – 30mm diameter.
Pualco Tillite *(Early Sturtian)*	This formation is a massive light to dark grey or green matrix supported tillite. The matrix has silt to sand sized grains that are generally sub-rounded and include; pegmatite, brown weathering dolomite, white quartz dominated granites, and pyritic quartz chlorite gneiss. Clasts commonly measure from 4 – 60 mm in diameter, occasionally up to 40cm diameter.	Some zones of the matrix are slightly more red than the published definition and a field example found at 289000E 652200N (Dalgarno 1965, Dalgarno 1966)

	Name	Published description	Additional characteristics observed in the field
Diapir Lithologies *(Willouran age evaporites of the Callanna Group*	Diapiric Breccia (DB)	Carbonate cement supports brecciated rock fragments of all sizes. Rafts have been documented within this lithology in the Oraparinna Diapir at greater 1km in diameter.	Well-cemented grey yellow gritty calcareous matrix. No individual grains discernible to the naked eye or with hand lens (10x magnification). Clasts vary in size from a few mm to the majority, which are 10 – 80mm diameter. Clasts are mainly grey or yellow competent sand and shale, with similar composition to the matrix. The northern margin of the diapiric breccia in the mapping area features zones of close to 100% dolomite, which shows well-formed manganese dendrites. Dolomite abundance decreases across the diapir body towards the south. Halite casts (cubes up to 8mm across) are present in some sandstone clasts. Anhydrite crystals have grown freely within open fractures in the diapiric breccia, particularly on the northern margin of the diapir adjacent to the Holowilena Ironstone (Figure 8)
	Brecciated Red Shale (BRS)	Diapir breccia with a red shale matrix.	Fine white carbonate cement forms the matrix This cement is softer and more readily weathered than cement of DB. Broken blocks of red shale around 4cm diameter dominate clasts. Shale clasts weather to green, yellow and white in some areas. Brecciation intensity increases to the west where the unit is at its thinnest. In the east brecciation textures are replaced by tight folds (figure 13)

Figure 5 A) Holowilena Ironstone featuring a sandstone band with ripple structures and cross beds B) Etina Formation with diapiric debris of sandy limestone. These clasts become larger with proximity to the diapir. (Locations shown in Figure 8)

METHODS

Formation boundaries were mapped in the field area and structural data was collected from lithologies proximal to, distal to and inside the diapir. (MGA94 Zone 54J 282400E 6534100N-2845250E 6532200N).

Fieldwork was carried out through detailed cross sections with a specific attention to tectonic factors including; discordant bedding relationships, unconformities and size and abundance of locally derived clast material that may be related to diapirism. Global Positioning System (GPS) location data in conjunction with spatial relationships to landmarks were used to generate a map on an aerial photograph of the Oraparinna area supplied by the Geological Survey of South Australia. Satellite images were used for contextual interpretation, and to extrapolate small-scale observations into their regional environment. Field data was correlated with drill core observations from the Blinman 2 drill hole, 1.5 km NNE of the Blinman Diapir.

OBSERVATIONS AND RESULTS

The Enorama and Oraparinna Diapirs are located in a north-south striking antiform structure, which begins near the eastern margin of Wilpena Pound, and extends to the north through the Blinman Diapir. All of the field observations and drill core observations in this document were from formations directly affected by this structure. The field map (Figure 8) features the diapir weld as it thickens into the body of the Enorama Diapir to the northwest. Outside of the diapir, stratigraphic thicknesses were generally uniform with bedding dipping away from the diapir toward the north and south. This data was collected from outcrop, formations (excluding the Sunderland

Formation, DB and Tapley Hill Formation which show significant resistance to weathering) cropped out best in creek beds and drainage channels.

Stratigraphy

Table 1 shows published descriptions. However additional and different characteristics have also been observed. These are presented in Table 1 also.

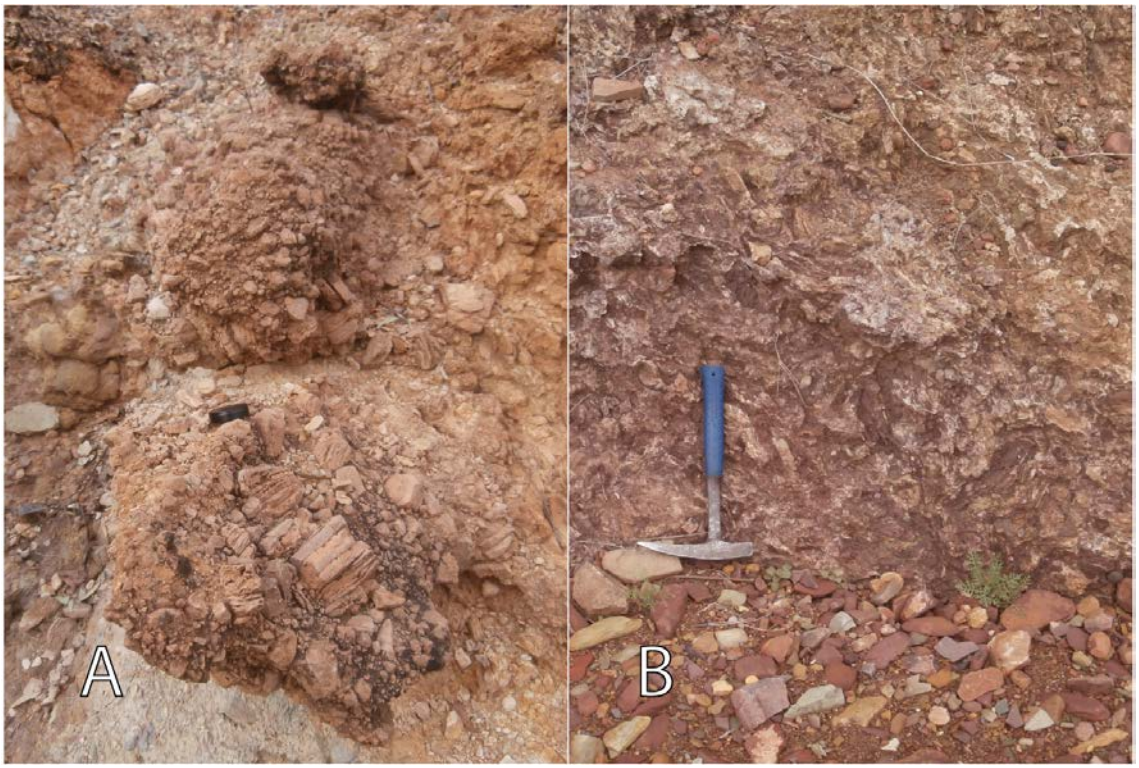

Figure 6 Diapiric breccia units, A) Diapiric Breccia (DB) B) Brecciated Red Shale (BRS) (locations shown in Figure 8)

Figure 7 Anhydrite crystals within the Diapiric Breccia (Location shown in Figure 8)

Diapiric Breccias of the weld

DIAPIRIC BRECCIA (DB)

There is a thin band as little as 10 cm of yellow matrix Diapiric Breccia (DB) between the Brecciated Red Shale (BRS) and the adjacent lithology to the southwest. This band is present from the south-eastern margin of the diapir in the mapping area before BRS thins, across the mapping area (Figure 8). It is always present when outcrop exists between the BRS and Sunderland, and between the BRS and Etina formations (Figure 8).

Figure 8. (A3 foldout) Geological map showing the weld between the Enorama and Oraparinna Diapir and their effect on the surrounding strata. Dotted lines indicate boundaries that have been defined by extrapolating interpretations from other outcrops. Lineation data with ^ indicates that the direction of movement may be 180° from that shown due to uncertainty in interpretation at the outcrop. Bedding plane data with * indicates that the block is thought to have slumped due to salt withdrawal, and is therefore discordant with adjacent data. The inset maps show the location of the mapping area in relation to the Flinders Ranges National Park, major roads and towns. Location information is included for figures 5,6,7,10,12,13, and 14.

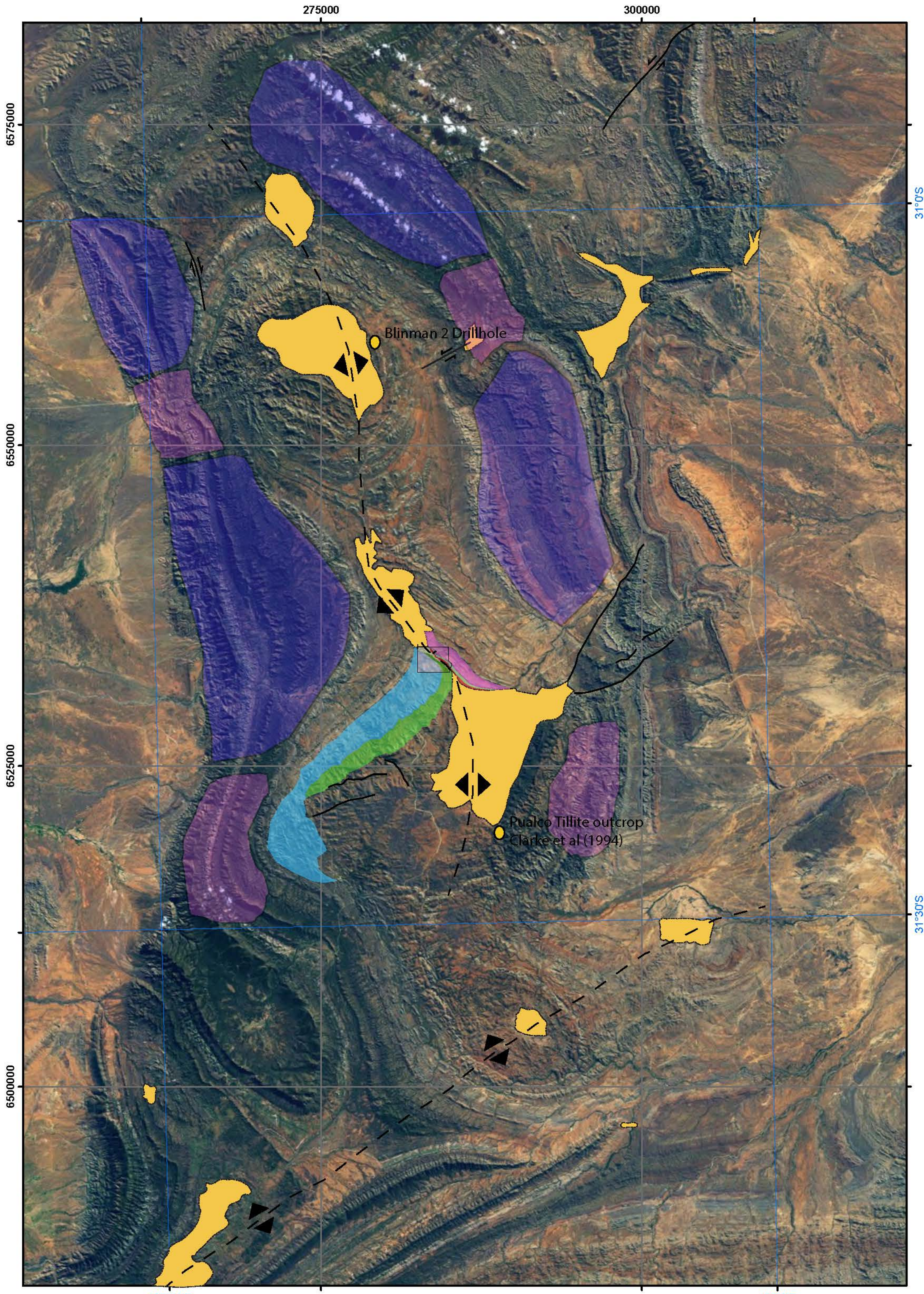
275000
300000
6575000
6550000
6525000
6500000
31°0'S
31°30'S
138°30'E
139°0'E
Blinman 2 Drillhole
Pualco Tillite outcrop
Clarke et al (1994)

BRECCIATED RED SHALE (BRS)

The BRS crops out along the length of the south-western margin of the diapir (Figure 8). This lithology has not previously been described across the mapping area. It has been described in relation to reef structures at the northern end of the Enorama Diapir (documented as 'diapir breccia red shale matrix' in Lemon 2011). The BRS is significantly more reactive to HCl than DB. More intense brecciation has occurred where the brecciated red shale is thinnest. Where the unit is thicker it is characterised by an intense folding instead of the breccia texture characteristic further west, and a less intense reactivity to HCl (Figure 12). Zones of intense folding showed bedding planes and bands of red and green alteration. These colour bands cross cut the bedding planes. In some areas the green bands have been extensively leached of Fe and organic material and are yellow or white.

A thin band of BRS occurs outside the diapir within the Sunderland Formation. The strike of this BRS unit is discordant to the Sunderland Formation forming a low angle difference. The material has a diapiric texture identical to the BRS contained within the diapir 150 m to the northeast. The contact between the Sunderland Formation and BRS is sharp, no clasts of the Sunderland Formation are present in the BRS, nor are clasts of BRS present within the Sunderland Formation.

DIAPIR RAFTS

Large rafts of non-evaporite material are observed within the diapir and in several cases outside, overlying stratigraphy adjacent to the diapir (Figure 9). Rafts observed in the field area are significantly smaller than others mapped in larger diapir bodies of the area (Dalgarno 1965, Dalgarno 1966). Previous mapping in the area has only documented

two types of diapir rafts; 1) amygdaloidal basic volcanics (Dalgarno 1965, Dalgarno 1966, Mawson 1942, Preiss 1987) and; 2) sedimentary rafts of the Callanna Group (Clarke 1994, Dalgarno 1965, Dalgarno 1966). This study has further differentiated these rafts due to the great variety of lithologies that are represented at the scale of field mapping undertaken.

Seven different types of diapir rafts were observed in the field area (figures 8 and 9). Rafts located outside of the diapir are only shown in Figure 9.

1) Type 1 rafts (R1) are massive, homogenous, orange, grey, medium-to coarse-grained clast supported competent sandstone. Carbonate content is absent. These rafts weather to cubic orange blocks, which is characteristic in the field.
2) Type 2 rafts (R2) are white and pale orange, calcareous shales and silts interbedded with sand layers. Sand layers are up to 6cm thick and shale layers are up to 1.5 cm thick. Some carbonate is present.
3) Type 3 rafts (R3) are basic volcanics. These have been correlated with the Wooltana Volcanics of the Arkaroola Subgroup (Mawson 1942, Preiss 1987). They are homogenous and grey with amygdales 1-3 mm diameter. Significant shearing and stretching of these basalt rafts has occurred along the south-western margin of the diapir (Figure 8).
4) Type 4 raft (R4) are composed of altered homogenous black ironstone and some 3-5 cm thick lenses of jasper. No discernible grains or bedding planes present at hand lens (10x) magnification. Specific gravity relative to adjacent shales and sandstone units is high.

5) Type 5 rafts (R5) are pink and purple siltstone with very low carbonate content, well-cemented matrix with dark lithics throughout.
6) Type 6 raft (R6) are red, orange matrix sandstone with fine to coarse grains of grey and orange colour (up to 2.5 mm diameter) and no carbonate content. Black bands of organic material on the lee slopes of ripples define cross bedding.
7) Type 7 rafts (R7) are made up of yellow and white calcareous shales, which alternate in layers 1-3 m thick. Fine to coarse sandy quartz bands occur throughout, and are up to 3 cm thick. Quartz crystals are rounded, well sorted and glassy.

Legend

- Inclined bedding strike and dip
- Overturned bedding and dip
- Slicken line lineation and plunge
- Fracture plane orientation
- Cleavage plane orientation
- Fault-arrows indicate displacement
- vertical dipping bedding plane
- Data adjacent to map area (Location marked in parentheses)
- Younging direction (upwards)
- Inferred boundary
- Diapir boundary

Diapir Rafts

- R1 Callana Group - orange sandstone
- R2 Callana Group - orange silts and sand interbeded
- R3 Wooltana Volcanics - Basalt
- R4 Altered Iron siltstone
- R5 Pink and Purple siltstone
- R6 Deformed bedded orange sandstone
- R7 Callana Group - yellow whilte shale with quartz bands

Lithological Units

- BRS Brecciated Red Shale
- DB Diapiric Breccia
- E Etina Formation
- S Sunderland Green Shale
- T Tapley Hill Formation
- W Wilyerpa Green Shale
- H Holowilena Ironstone
- P Pualco Tillite

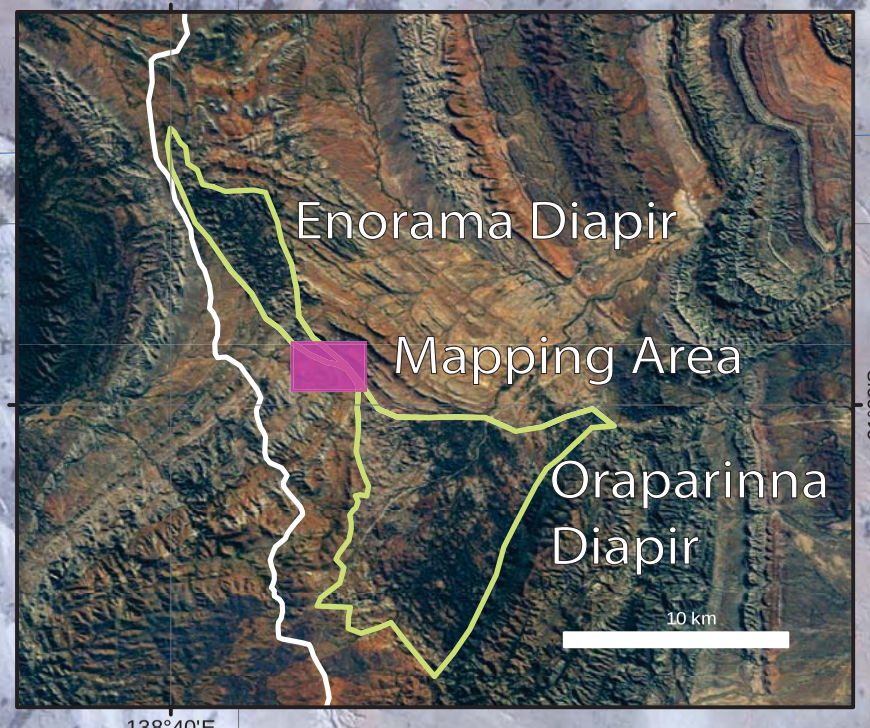

N

GDA 94 Zone 54
Mag. Dec. (2013) 7°25"E

New Stratigraphy

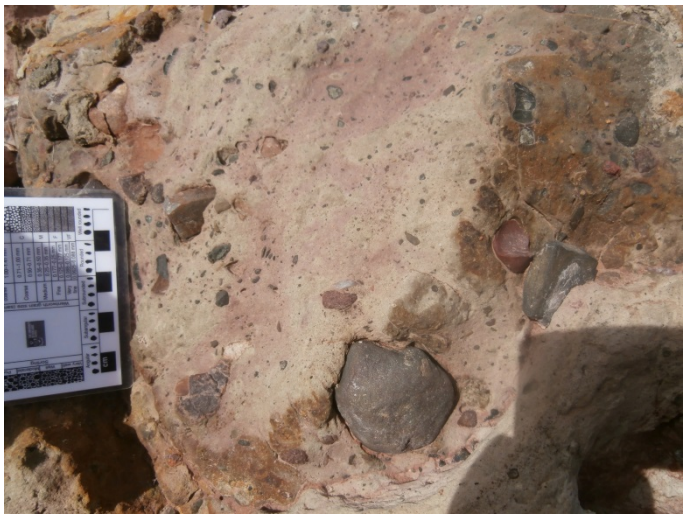

Figure 10 Pualco Tillite of the field area. The matrix here is slightly redder than that of the Pualco Tillite south of the Oraparinna Diapir. Clasts shown are metapelites.

Stratigraphy on the northern side of the diapir begins at the diapir margin with a small lens of Pualco Tillite, which has not been previously described in contact with the diapir weld in this location (Figure 10). The nearest documented location is 289000E 652200N on the southern margin of the Oraparinna Diapir 10 km to the south (Figure 17). Samples that cropped out at the weld were compared with rocks from this location, and the description by Clarke (1994). In the field area the Pualco Tillite was found at 284303E 6533209N and extends to 284353E 6533204N along a creek bed orthogonal to the diapir margin (Figure 8). The northern and southern margins of this unit are buried below regolith. The matrix of the Pualco Tillite in this location is grey, blue and red in colour, but is slightly redder than the reference sample from south of the Oraparinna Diapir (Figure 17).

Structural Data

Bedding planes south of the diapir have steep to shallow dips towards the southwest, including 4 overturned beds adjacent to the diapir. This trend is relatively strong. North of the diapir, a weaker trend shows bedding planes dipping towards the northeast including 8 overturned beds adjacent to the diapir. Bedding plane data from within the diapir was not systematic.

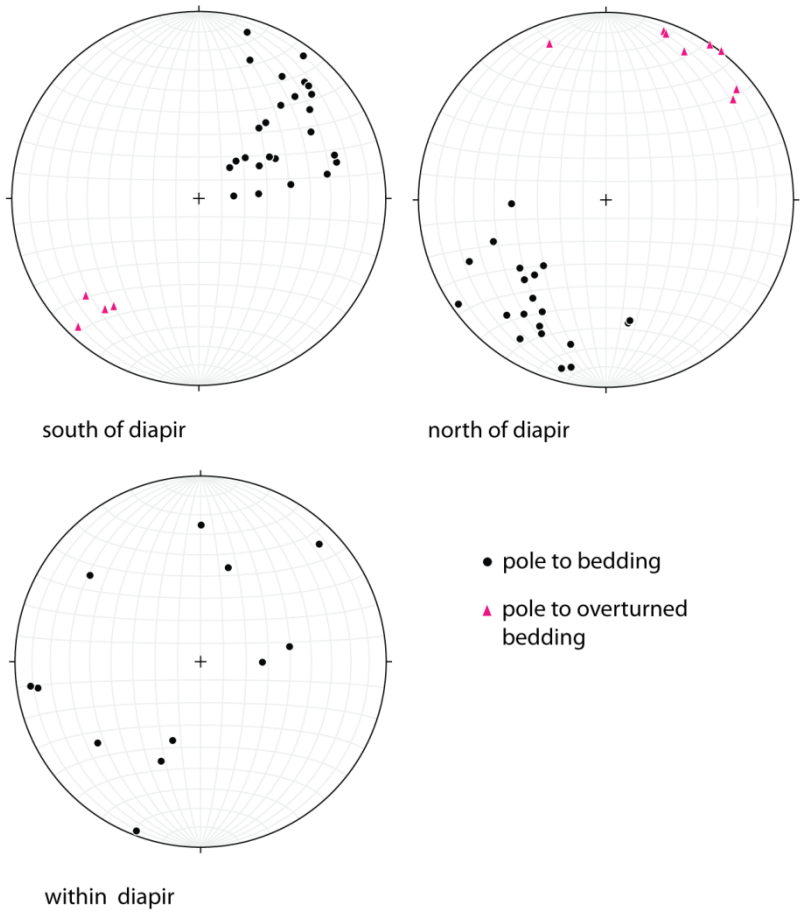

Figure 11 Poles to bedding planes within and on each side of the weld. Data from south of the diapir is the most concordant, and occurs in the youngest stratigraphy. Less concordant is the data from the north. The oldest and most disturbed material is the diapiric breccia and is represented by the discordant dataset within the diapir.

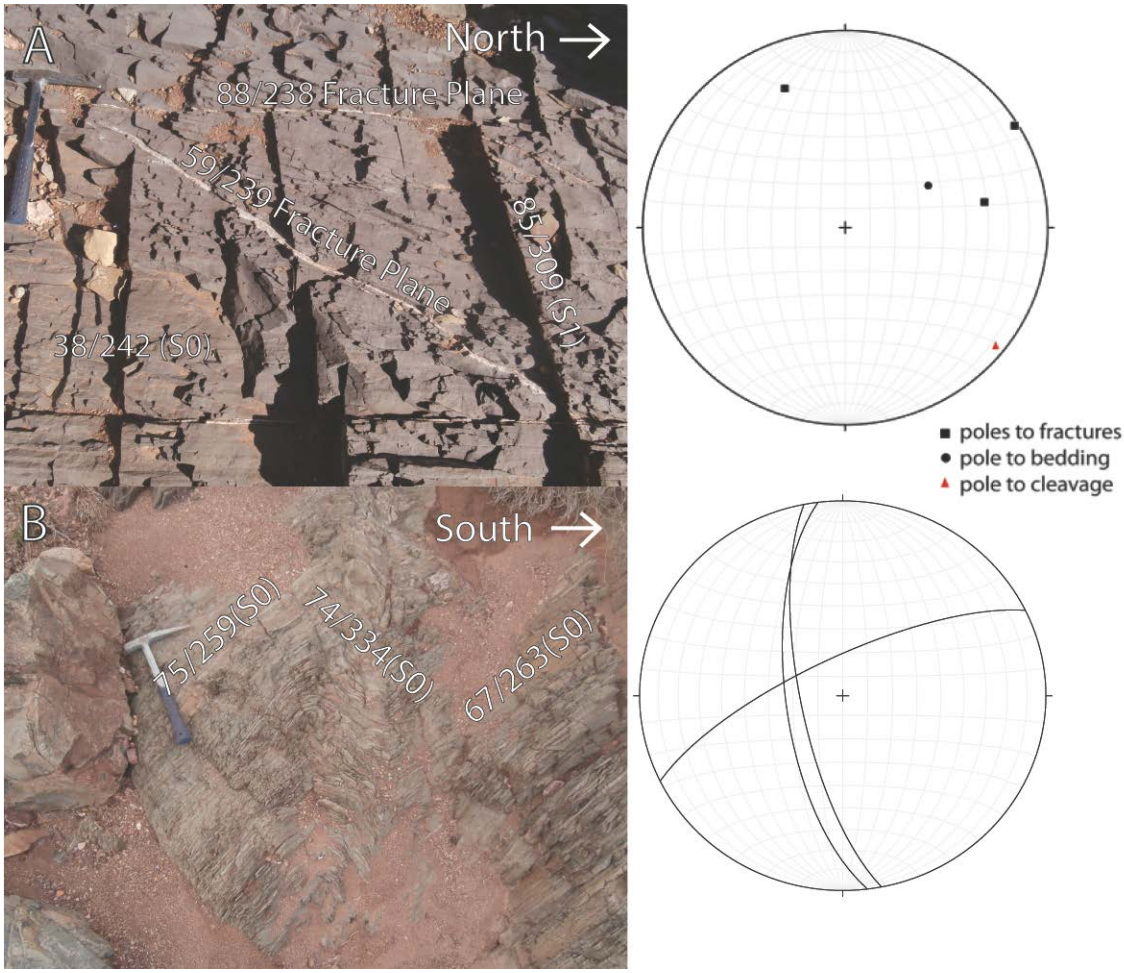

Figure 12 In parentheses is the structural fabric which the plane data (dip/dip direction) refers. A) Shows a late stage of deformation in the youngest lithology of the mapping area (Etina Formation.) B) shows the tight folds of BRS, these planes are plotted as great circles (locations shown in Figure 8).

Location 12b is a zone of the BRS, which has not been brecciated and is expressed by the tight folds shown. This occurs in the eastern end of the mapping area where this unit's thickness is greatly increased (Figure 12b). The bedding planes shown in the stereonet of Figure 12b show: 1) dip to the north-northwest and 2) dip to the west. The intersection of these planes shows a fold hinge dipping steeply (~70º) toward the west-northwest (Figure 12b).

Fractures at location 12a cannot conclusively defined as conjugate pairs, and therefore cannot be linked to each other through a single tectonic event. However, due to their

proximity and lack of cross cutting and offset, their relationship to a common tectonic event can be inferred as neither fracture has cut, offset or destroyed the other (Figure 12a).

Fractures planes and slicken lines of the Tapley Hill Formation measured at 283559E 6534210N indicate a southerly transport direction (Figure 13). Each of the sheer planes with slicken lines features a stepping texture indicating a transport direction toward the south.

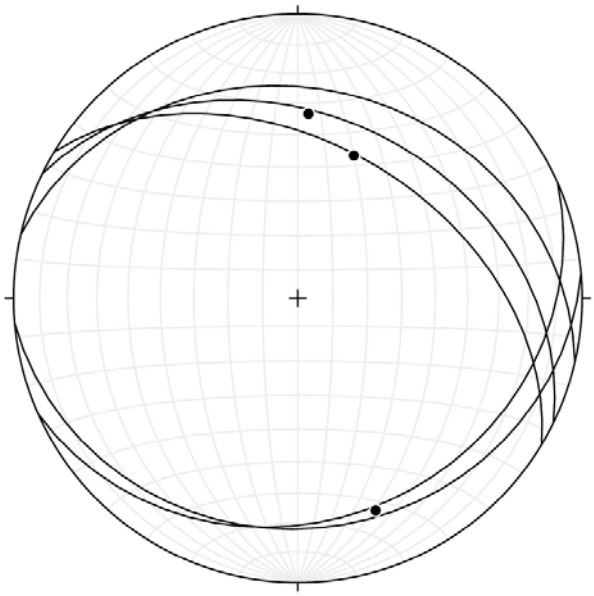

Figure 13 Great circles represent fracture planes measured at 283559E 6534210N in the Tapley Hill Formation. Points represent trend and plunge of slicken lines measured on the planes that they intersect in the plot. All of the slicken lines in this location features a stepping texture which indicates a transport direction toward the south.

Two sinistral fault structures have been mapped striking orthogonal to the northern diapir margin (Figure 8). Neither of these structures persist across the diapir.

Fault 1 is the larger inferred fault at the northern end of the mapping area. It places the Wilyerpa Formation adjacent to the Tapley Hill Formation. Thirty metres downslope, underneath the Wilyerpa Formation, the Holowilena Ironstone crops out. Adjacent to

this location under the Tapley Hill Formation, the Holowilena Ironstone is absent, reappearing 30m downslope. Thus supporting the 30 m dextral displacement mapped for Fault 1 (Figure 8).

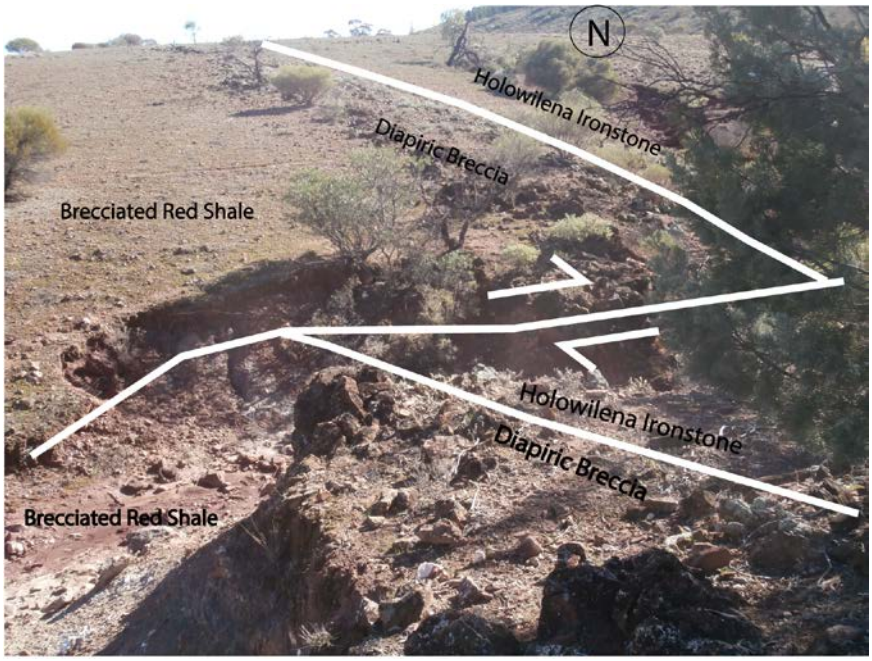

Figure 14 fault 2 in the centre of mapping area (Figure 8). This fault displaces DB by 8m.

Fault 2 strikes along a creek bed, and places DB adjacent to the Holowilena Ironstone with an 8 m dextral displacement (Figure 14). No displacement was observed at the boundary of the Holowilena Ironstone and Wilyerpa Formation, nor the boundary of the Wilyerpa Formation and Tapley Hill Formation.

Stratigraphic thickening of the Holowilena Ironstone occurs on the north-western side of Fault 1, before the unit pinches out at the Wilyerpa Formation-DB contact. Thickening also occurs in the BRS at the south-eastern end of the diapir in the mapping area, as the DB thins causing the diapir weld to retain its width of 100 m.

Blinman 2 Drill Core

Frontier Resourced Ltd drilled Blinman 2 to 2031.45m in 1991. The drill hole is located at 279900.76E 6556778.39N approximately 1.5 km NNE of the Blinman township (SA Geodata, 2013).

The aim of this drilling project was to intersect the diapiric breccia of the Blinman Diapir, however it did not reach it at the anticipated depth and the drilling was abandoned (Weste 1991). The bottom 50 m (1981 – 2031.45 m) of the drill hole feature tillite facies of the Wilyerpa Formation (Weste 1991). The core was investigated in this study in order to make a comparison to field outcrops (Figure 15). The core was not oriented; therefore, the following observations do not include structural data.

Sediments in the core show a dynamic environment with an oscillating environmental change between a low energy environment, where muds were deposited, and a higher energy environment, where sands were deposited. Clasts are made up of laminated shale and mudstones up to 15 cm in diameter, many of which are 1-2 mm in diameter (Figure 15a). Quartzofeldspathic granite clasts are also present. These are less common and tend to be quite large; some intersecting up to 40 cm of core.

A degree of mixing of mud and shale components of this rock has occurred. Mixing has a character of gentle soft sediment slumping, prior to lithification and significant burial (figures 15a, b and c). A shear fabric is also present, with small fractures filled with a mud matrix. This shear fabric texture occurs around larger clasts, up to 5 cm in

diameter, which have been imbricated, demonstrating the sheer strain orientation (Figure 15c). This fabric is present only in short sections of drillcore (Figure 15d).

Figure 15 A) shows sand and shale clasts being deposited on a shale layer B) sand and shale mixing C) abundant clasts among shale and sand layers D) sheer fabric.

Diapiric Breccia

Variation in the concentration of carbonate material is consistent with an increased amount of water passing through some parts of the diapir and dissolving the salt material, which was once present. This water will also dissolve the soluble carbonate minerals of the bulk carbonate content. The presence of large anhydrite crystals in fractures of DB (Figure 7) indicate that this material did not lack accommodation space when salts were being precipitated and gypsum dehydrated. Anhydrite has previously

been associated with diapir bodies and their cap rocks when the salt have been removed by surface water (Saunders and Thomas 1996). Anhydrite in this location indicates that loss of salts and alteration of gypsum has occurred in this location.

An increase in water movement on the southern side of the diapir weld is consistent with the model of secondary diapirism (Figure 16). Increased movement of material, and intense brecciation seen both in the BRS and DB at the southern margin of the diapir would dynamically create and destroy pore spaces. Allowing salt material to have contact with meteoric water sources, hence more rapid dissolution (Saunders and Thomas 1996) than with DB on the less active northern side of the diapir (Figure 8).

Brecciated Red Shale

Brecciated Red Shale is least deformed at the eastern end of the mapping area closest to the Oraparinna Diapir source. Structural controls on salt movement have restricted the movement of BRS causing thinning and stretching of the unit throughout the growth of the secondary diapir structure. The fact that thinning has occurred to the extent shown (Figure 8) indicates that this unit was considerably more ductile and mobile relative to the rest of the DB in this area (Figure 8).

The breccia texture, calcite veining and alteration that characterises the majority of BRS in outcrop are more prevalent at the thinnest part of this unit, which is closest to the Enorama Diapir in the north-west (Figure 8). This thinning and brecciation, as opposed to the tight folding observed in this lithology to the east, indicates a difference in rheological behaviour to the DB when affected by the stress that has acted upon the diapir. The interpretation of these outcrop expressions is that the breccia texture

represents a similar amount of movement to the tight folds, concentrated into a smaller space, hence a more localised and intense deformation. The difference in yield strength between the DB and BRS observed in outcrop supports this interpretation (Figure 6).

A thin band of BRS is located within the Sunderland Formation near the centre of the mapping area. The material strikes across, at a low angle, the strike of bedding of the Sunderland Formation. This represents a period of erosion at the surface of the diapir within the time period that the Sunderland Formation was deposited. This lens marks a shallow band of collapsed material of BRS from the cap of the diapir, which has been subsequently preserved within the Sunderland Formation. This material is not a raft deposited by the diapir; because it is far less competent and dense than nearby rafts. Nor does it have a large round shape that would resist weathering of material of its interior. A thin weak raft would not resist weathering and erosion over this length of time.

EVOLUTION OF THE ORAPARINNA AND ENORAMA DIAPIRS

Previous work has discussed growth faults and thrusts (Lemon 1988) and displacement of the basement (Backé et al. 2010). Discussed below is a model based on differential loading for diapir development which does not require such large-scale faulting.

The first recorded diapirism in the mapping area was in the early Sturtian, when the Pualco Tillite was being deposited (figures 10, 16a and b). At this time an extensional tectonic regime was dominant and salt was mobilised due to an extensional fault, which went on to form the nucleus of the Oraparinna Diapir body (Figure 16a). Sedimentation

continued, enhancing the differential load and causing a minibasin to form to the north-east of the locus of diapir initiation. This minibasin formed around the initial site of increased load as the relatively dense sediment forced the mobile salt out from below. This created more accommodation space for subsequent dense sediment (Figure 16c). When the salt was depleted under the initial minibasin and the minibasin is filled, the next available depocentre will be on the opposite side of the diapir as described by flip flop tectonics (Quirk 2012) (Figure 16d). This occurs when there is no longer any mobile salt underneath the minibasin (Quirk 2012). The older sediments to the north have steeper dips, due to a longer history of minibasin growth, which has continued to bend and distort this stratigraphy as younger sediment fills the space created by mobilised salt. This minibasin was filled at the end of the Sturtian after the end of the Tapley Hill Formation deposition. Subsequent sedimentation will occur in a wider area until another fault grows, allowing the growth of another minibasin (figure 16 d and e). Faults dipping toward the basin have been shown to nucleate diapir growth in this manner in the Gulf of Mexico (Rowan et al. 1999). In this case another zone of potentially mobile salt lies under the opposite side of the growing diapir, which is likely to be the weakness to become the next minibasin (Figure 16d). This second minibasin coincides with the majority of growth of the secondary Enorama Diapir and includes the Sturtian-Marinoan boundary.

Further extension results in the formation of normal faults near the crest of the diapir at the weakest points of the structure (Vendeville 1992b) (Figure 16d). Should the salt be sufficiently mobile, a second fault will be filled with salt and a secondary diapir will form, in much the same manner as diapirism was initiated (Figure 16e). Secondary

diapirism has occurred in extensional faults at the crest of established diapirs in the manner described above, in the North Germany Basin (Warsitzka et al. 2013). Similarly, two small secondary diapirs have grown above what used to be one large salt body in the La Popa Weld of the Gulf of Mexico (Rowan et al. 1999, Fort 2012). This occurred as a result of salt of from larger primary diapir being depleted, subsequent collapse of adjacent strata forces the remaining salt into two smaller diapirs at the edge of the original diapir (Fort 2012). The shape and form of this secondary diapir will be determined by structural weaknesses, initially following the fault that allowed its initiation. This can lead to the development of salt nappes and salt glaciers (Ferrer 2012). A small part of the north-western Enorama Diapir did reach the surface during the late Sturtian when the Etina Formation was being deposited. Salt glaciation is evident where stromatolite reefs growing on BRS on north western Enorama Diapir (Lemon 2011).

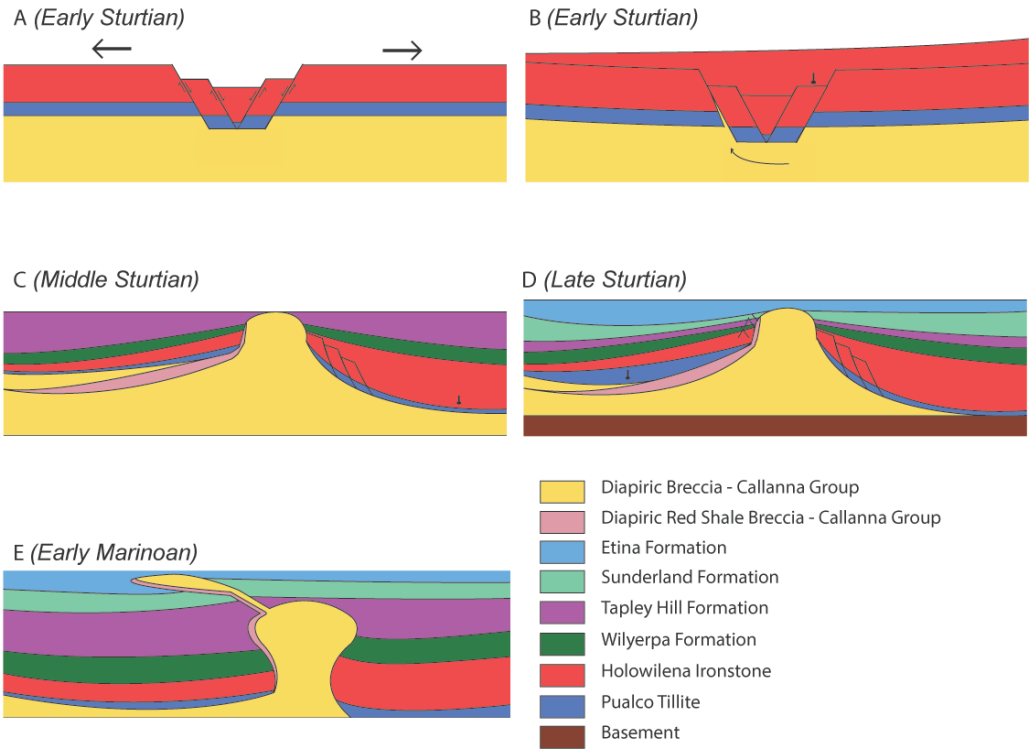

Figure 16 model of diapir growth. A) Initial extensional environment. B) Uneven loading due to increased sedimentation on the right of the image causing flexure and minibasin growth, and the beginning of diapirism. C) Diapir growth with uneven sedimentation on each side of the diapir due to differential loading. D) Further extension causes faulting near the crest of the diapir, and depletion of evaporites under the minibasin causes a new minibasin to grow on the opposite side of the diapir. E) Secondary diapir forms in the extensional faults of phase D. Movement of evaporites on this side of the diapir sees movement of the brecciated red shale mobilised into the left side of both the primary and secondary diapirs.

REGIONAL CONTEXT

The Blinman, Enorama and Oraparinna Diapirs align north to south in the Flinders Ranges along the hinge of an antiform (Figure 17). This demonstrates outward dipping material younging away from the breccia bodies. It is likely that these diapirs have caused the formation of this antiform, this is consistent with fold formation in the La Popa Basin, Northern Gulf of Mexico (Rowan and Vendeville 2006). Growth of the Blinman and Oraparinna diapirs has caused relative topographic highs during the Sturtian to the area between them, hence the Sturtian and Marinoan sediments have

been deposited in much greater thicknesses in this area. The presence of the Enorama Diapir within this thick sequence of sediment indicates that the Enorama Diapir has been injected into an older minibasin, which formed during primary stages of Blinman and Oraparinna Diapir development.

Blinman 2 drillcore observations indicate that diapirism in the Blinman Diapir was active at the time of Wilyerpa Formation and Tapley Hill Formation deposition (Middle Sturtian). A significant topographic high was present at the crest of the diapir causing diapiric debris to collect in the minibasin, this indicates that the Blinman diapir was both active and proximal to the diapir at the time of middle Sturtian deposition. Diapiric debris is common surrounding diapir domes, documented in the Gulf of Mexico and the North German Basin (Warsitzka et al. 2013, Girardi 2012). Soft sediment deformation indicates a dynamic environment of topographic relief and abundant sediment, which is consistent with active diapirism. Mud filled sheer fabric textures are likely to be a product of a mud with a high cohesive strength enabling brittle fracture, to be then filled muddy fluids. This is likely a consequence of lower cohesive muds being fractured as a result of minibasin flexure and rotational stress, and subsequently injected with younger mobile muds from above.

Figure 17 – (A3 foldout) Regional Map. Purple shading indicates sediment thickening, pink shading indicates sediment thinning.

Replace this page with a colour A3 printout of the Regional Map

Strike slip faults with large sinistral displacements, are observed in the north-eastern corner at 6576000E and 30000N and across the Bunkers Graben. West of the diapir antiform (Figure 17), displacement is minimal, indicating that much of this strain has been absorbed by the diapir structures due to salt withdrawal.

The movement of the Bunkers Graben in the middle Cambrian occurs in a west-southwest direction, which is oblique to the boundaries of the sinistral strike slip deformation zones active at the time. This indicates that they are consistent with 'En-Echelon Faulting' (Fort 2012). These faults occur in an environment where a thin skin of sediment overlies a salt body and the sediment expresses a degree of rotation before it becomes a series of small faults oblique to the overall direction of movement. The subsequent strike of the small faults is 20 – 50° oblique to the regional strike slip displacement (Fort 2012).

Fracture planes and slicken lines observed in the Tapley Hill Formation indicate a transport direction towards the south (Figure 13). This is likely associated with salt withdrawal and movement of the Bunkers Graben, due to the direction of movement indicated by 'En-Echelon Faulting' being consistent with the slicken lines observed. This transport direction is consistent with large-scale fault movements observed to the east and north-east of the Blinman Diapir (Clarke 1994, Dalgarno 1965, Dalgarno 1966, Rowan and Vendeville 2006)

Rafts outside the diapiric breccia

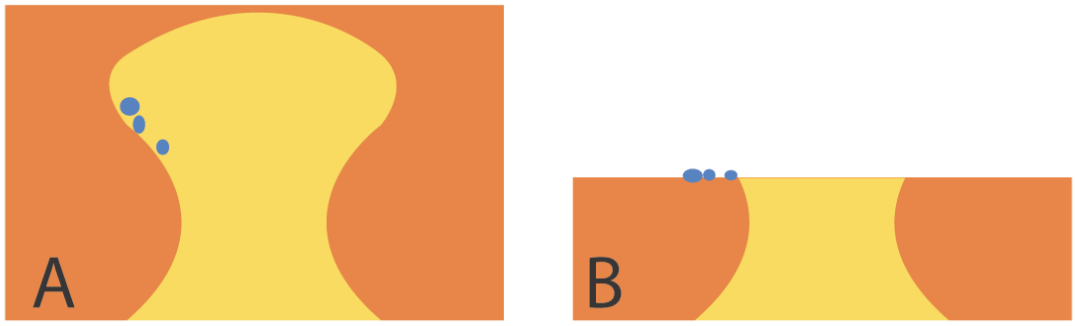

Figure 18 A) Diapir with rafts (blue) submerged in adjacent stratigraphy. B) The same diapir after limited further diapirism and significant erosion. The rafts are more resistant to erosion than the surrounding strata and the diapiric breccia.

Rafts are mainly located on and near the southern edge of the diapir weld including several that have been observed outside the diapir itself (Figure 9). For this to occur a significant amount of erosion is required to have taken place (Figure 18). The rafts are highly competent relative to the diapiric breccia, which is weaker and more likely to be eroded, thus leaving the rafts at the surface after erosion. This is consistent with the tendency of many of the rafts mapped to form topographic.

Provenance of the majority of rafts is uncertain. However, R3 the volcanic rafts, have been correlated to the Wooltana Volcanics of the Arkaroola Subgroup on multiple occasions; first by Mawson (1942) and supported since by Preiss (1987). Comparison of other rafts with material forming the diapiric breccia indicates that some of them are composed of similar material and may have the same provenance in the Curdimurka and Arkaroola Subgroups. Raft types 1 and 6 resemble sandstone components of the diapiric breccia. Raft types 2 and 7 resemble the weathered red and white zones of the BRS. Raft type 7 forms a similar elongated shape to the BRS itself, which may indicate that it has been deformed in a similar manner. Rafts 3, 4 and 5 do not resemble anything observed within the diapir body. All of this material is thought to come from material

deposited between evaporite layers, which have subsequently been mobilised with surrounding material.

Due to their size, and amount of movement that has occurred, it is certain that these rafts were lithified and brittle at the time they were mobilised within the DB. Therefore, a significant amount of time must have passed before they were affected by diapirism. Rafts are more prevalent on the southern side of the diapir than on the north where the initial minibasin was located, hence allowing more time for lithification and brittle characteristics of the raft material to occur. This is a likely explanation for the increased abundance of rafts to the south, the more recently active part of the diapir.

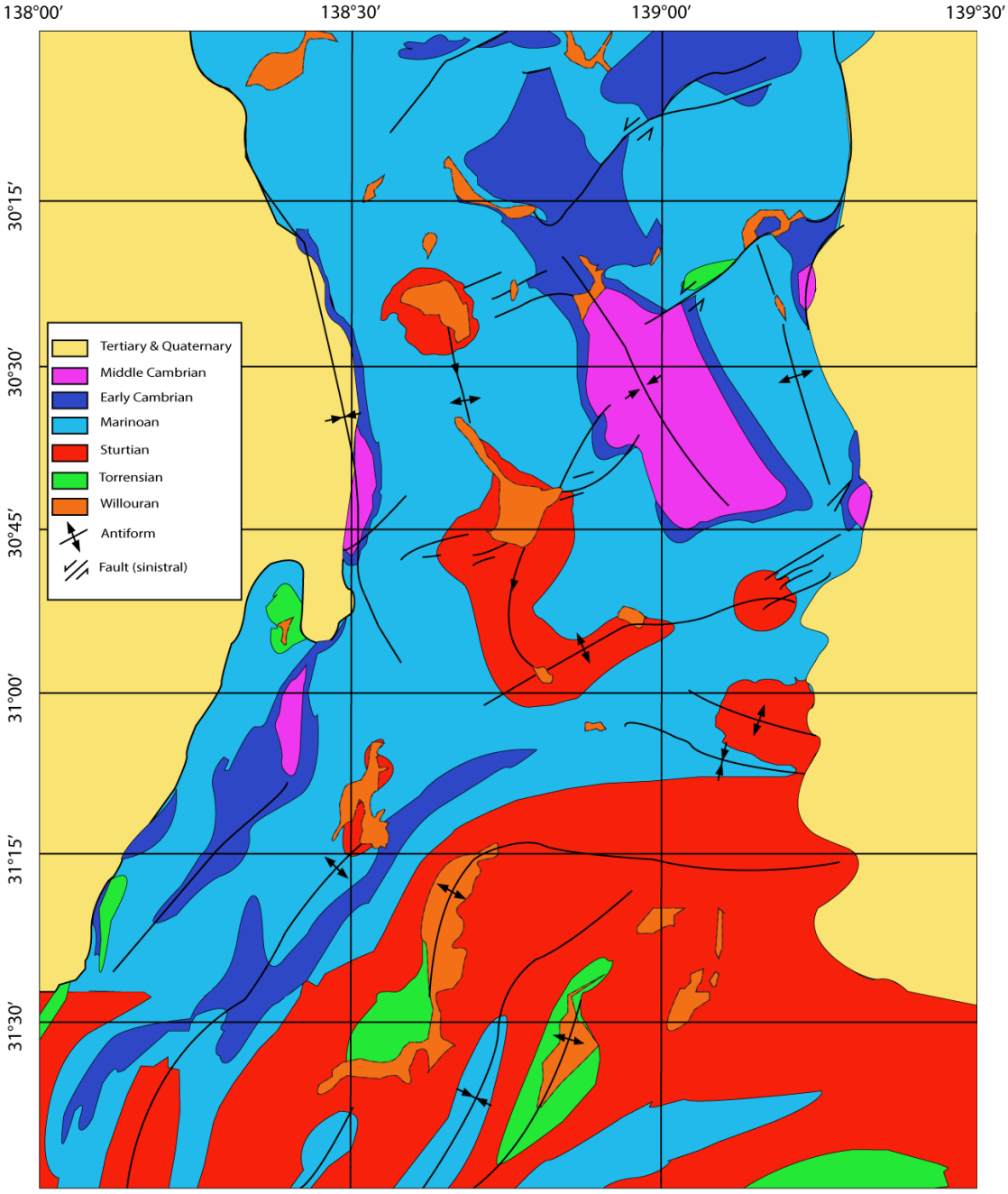

Figure 19 Tectonic Sketch of the central Flinders Ranges adapted from (Dalgarno 1965, Dalgarno 1966). Willouran sediments in this image are diapirs.

The north-south trending antiforms observed in the Flinders Ranges are the dominant structures in the area (Figure 19). This means that throughout the Sturtian, Marinoan, and into the Cambrian, the dominant maximum stresses have been striking generally north-east, south-west. An anticlockwise rotational strain is the cause of the increased

displacement in the northern extreme particularly in the sinistral strike-slip faults east of the Blinman Diapir structure and across the Bunkers Graben (Figure 19). There is a lack of significant faults in any orientation adjacent to the Enorama Diapir, which indicates that the strain has been absorbed by the movement and deformation of the diapir structure and the relatively soft diapiric breccias as material has moved west, which is consistent with movement shown (Figure 19).

CONCLUSIONS

The smaller scale of this mapping project has led to a new perspective on the Enorama and Oraparinna Diapirs and the weld that connects them. Previous work has discussed growth faults and thrusts (Lemon 1988) and displacement of the basement (Backé et al. 2010). Neither of these conclusions has been discounted; however field relationships including the lack of definitive thrust faulting in outcrop has led to a differential loading model presented in this body of work (Figure 16).

Additionally the stretching and change of character of the BRS along the western margin of the Enorama Diapir documents a stress environment consistent with development of a secondary diapir. Growth of a secondary diapir (the Enorama Diapir) into the edge of a pre-existing minibasin is supported by changes in sediment thickness adjacent to the diapir (figures 16 and 17).

Small-scale fieldwork in the area has also led to the documentation of a new stratigraphic relationship between the Pualco Tillite and the diapir weld (Figure 8). This addition to the evolution of the diapir indicates that the diapir was active prior to the deposition of the Holowilena Ironstone.

ACKNOWLEDGMENTS

Sincerest thanks are due to several staff and fellow students who have assisted with this project. Specific help and guidance has been in field work, peer reviews, and exchange of ideas.

Thanks go to: Dr Rosalind King, Bob Dalgarno, Dr Kathryn Amos, Lachlan Richards, John Waldon Counts, Nick Lemon, and Katie Howard.

APPENDIX

West and East Map files are copies of the hand drawn field map. See attached.

REFERENCES

ARCHER S. G., ALSOP, G IAN., HARTLEY, ADRIAN J., GRANT, NEIL T., HODGKINSON, RICHARD 2012 Salt tectonics, sediments and prospectivity: an introduction, *Geological Society of London, Special Publications,* vol. 363, pp. 1-6.

BACKÉ G.*, et al.* 2010 Basin geometry and salt diapirs in the Flinders Ranges, South Australia: Insights gained from geologically-constrained modelling of potential field data, *Marine and Petroleum Geology,* vol. 27, no. 3, pp. 650-665.

CLARINGBOULD J. S.*, et al.* 2013 Structural evolution of a salt-cored, domed, reactivated fault complex, Jebel Madar, Oman, *Journal of Structural Geology,* vol. 51, pp. 118-131.

CLARKE J. D. A., DALGARNO, C.R., DREW, G.J., DREXEL, J.F., DYSON, I.A., GRAVESTOCK, D.I., GUM, J., HARRIS, J.M., JANSYN, J., JOHNSON, J.E., LEMON, N.H., MORRIS, B.J., OLSEN, J., PREISS, W.V. 1994 Geology of the Flinders Ranges National Park. In CALLAN R. A., REID, P.W. ed. Adelaide: Primary Industries and Resources South Australia.

DALGARNO C. R., JOHNSON, J.E, 1965 ORAPARINNA Map Sheet 1:63 360. Adelaide: Geological Atlas of South Australia Geological Survey of South Australia.

--- 1966 PARACHILNA Map Sheet 1:250 000. Adelaide: Geological Atlas of South Australia Geological Survey of South Australia.

DREXEL J. F., PREISS, W.V. (EDS) 1995 The Geology of South Australia Vol. 2, The Phanerozoic. Geological Survey, South Australia.

DYSON I. A. 1996 A new model for diapirism in the Adelaide Geosyncline, *MESA - Mines and Energy South Australia,* vol. 3, pp. 41-48.

--- 1998 The 'Christmas tree diapir' and salt glacier at Pinda Springs, central Flinders Ranges, *MESA - Mines and Energy South Australia,* vol. 10, pp. 40-43.

--- 1999 The Beltana Diapir - salt withdrawal minibasin in the northern Flinders Ranges, *MESA - Mines and Energy South Australia,* vol. 15, pp. 40-46.

--- 2004 Geology of the eastern Willouran Ranges, *MESA - Mines and Energy South Australia,* vol. 35.

FANNING C. M., LUDWIG, K.R., FORBES, B.G., PRIESS, W.V. 1986 Single and multiple grain U-Pb zircon analyses for the early Adelaidean Rook Tuff, Willouran Ranges, South Australia. 8th Australian Geological Convention. pp. 71-72. Adelaide: Geological Society of Australia.

FERRER O., JACKSON, M.P.A., ROCA, E., RUBINAT, M. 2012 Evolution of salt structures during extension and inversion of the Offshore Parentis Basin (Eastern Bay of Biscay), *Geological Society of London, Special Publications,* vol. 363, pp. 361-379.

FORT X., BRUN, J.P. 2012 Kinematics of regional salt flow in the northern Gulf of Mexico, *Geological Society of London, Special Publications,* vol. 363, pp. 245-264.

GILES K. A., ROWAN, MARK, G.A. 2012 Concepts in halokinetic-sequence deformation and stratigraphy. In ALSOP G. I., ARCHER, S.G., HARTLEY, A.J., GRANT N.T., HODGKINSON, R. ed. Salt Tectonics, Sediments and Prospectivity. London: Geological Society

GIRARDI O. 2012 In-Situ Stresses and Paleostresses around Salt Diapirs: a Structural Analysis from the Gulf of Mexico and Amadeus Basin, Central Australia. The University of Adelaide.

JACKSON M. P. A. & VENDEVILLE B. C. 1994 Regional extension as a geologic trigger for diapirism, *Geological Society of America Bulletin,* vol. 106, no. 1, pp. 57-73.

JACKSON M. P. A., VENDEVILLE B. C. & SHULTZ-ELA D. D. 1994 Structural dynamics of salt systems, *Annual Review of Earth and Planetary Sciences,* vol. 22, pp. 93-117.

KERNEN R. A., GILES, K.A., ROWAN, M.G., LAWTON, T.F., HEARON, T.E. 2012 Depositional and halokinetic-sequence stratigraphy of the Neoproterozoic Wonoka Formation adjacent to Patawarta allochthonous salt sheet, Central Flinders Ranges, South Australia. In ALSOP G. I., ARCHER, S.G., HARTLEY, A.J., GRANT N.T., HODGKINSON, R. ed. Salt Tectonics, Sediments and Prospectivity. London: Geological Society

KING R.*, et al.* 2012 Stress deflections around salt diapirs in the gulf of mexico, *Geological Society of London, Special Publication,* vol. 367, no. 1, pp. 141-153.

LEMON N. M. 1985 Physical modeling of sedimentation adjacent to diapirs and comparison with late Precambrian Oratunga Breccia body in Central Flinders Ranges, South Australia, *American Association of Petroleum Geologists Bulletin,* vol. 69, no. 9, pp. 1327-1328.

--- 1988 Diapir recognition and modelling with examples from the late proterozoic Adelaide Geosyncline, Central Flinders Ranges, South Australia. University of Adelaide.

--- 2011 Interaction Between Sedimentation and Active Diapirism: Flinders Ranges. Student - Industry Field Trip. University of Adelaide AAPG Student Chapter.

MAWSON D. 1942 The structural character of the Flinders Ranges, *Trans. Royal Society South Australia,* vol. 66, pp. 262-272.

MOONEY M. D., COATS, R.P. 1981 The Blinman Dome "Diapir". In DIVISION G. S. O. A. I. S. A. ed. pp. 114-159. South Australia.

MOTAMEDI H.*, et al.* 2011 Multi-phase hormuz salt diapirism in the southern Zagros, SW Iran, *Journal of Petroleum Geology,* vol. 34, no. 1, pp. 29-43.

MOUNT T. J. 1975 Diapirs, Diapirism in the Adelaide Geosyncline, South Australia. University of Adelaide.

PREISS W. V. 2000 The Adelaide Geosyncline of South Australia and its significance in Neoproterozoic continental reconstruction, *Precambrian Research,* vol. 100, no. 1–3, pp. 21-63.

PREISS W. V., COATS, R.P., FORBES, B.G., 1987 The Adelaide Geosyncline-late Proterozoic stratigraphy sedimentation, palaeontology and tectonics. Geological Survey South Australia.

PRIESS W. V., BELPERIO, A.P., COWLEY. W.M., RANKIN, L.R. 1993 Neoproterozoic. In DREXEL J. F., PRIESS, W.V., PARKER, A.J. ed. The Geology of South Australia South Australia: Mines and Energy South Australia.

QUIRK D. G., PILCHER, ROBIN S. 2012 Flip-flop salt tectonics, *Geological Society of London, Special Publications,* vol. 363, pp. 245-264.

ROWAN M. G., JACKSON M. P. A. & TRUDGILL B. D. 1999 Salt-related fault families and fault welds in the northern Gulf of Mexico, *AAPG Bulletin,* vol. 83, no. 9, pp. 1454-1484.

ROWAN M. G. & VENDEVILLE B. C. 2006 Foldbelts with early salt withdrawal and diapirism: Physical model and examples from the northern Gulf of Mexico and the Flinders Ranges, Australia, *Marine and Petroleum Geology,* vol. 23, no. 9-10, pp. 871-891.

SAUNDERS J. A. & THOMAS R. C. 1996 Origin of 'exotic' minerals in Mississippi salt dome cap rocks: Results of reaction-path modeling, *Applied Geochemistry,* vol. 11, no. 5, pp. 667-676.

SCHOENHERR J.*, et al.* 2010 Deformation mechanisms of deeply buried and surface-piercing Late Pre-Cambrian to Early Cambrian Ara Salt from interior Oman, *International Journal of Earth Sciences,* vol. 99, no. 5, pp. 1007-1025.

UNKNOWN 2013 SA Geodatabase. Department for Manufacturing Innovation Trade and Energy.

VENDEVILLE B. C., JACKSON, M.P.A 1992a The fall of diapirs during thin-skinned extension, *Marine and Petroleum Geology,* vol. 9, pp. 331-353.

--- 1992b The rise of diapirs during thin-skinned extension, *Marine and Petroleum Geology,* vol. 9, pp. 331-353.

WARSITZKA M., KLEY J. & KUKOWSKI N. 2013 Salt diapirism driven by differential loading — Some insights from analogue modelling, *Tectonophysics,* vol. 591, no. 0, pp. 83-97.

WESTE G. 1991 Blinman 2 well completion report. Frontier Resources Ltd.